Bulk Scattering Properties for the Remote Sensing of Ice Clouds. Part I: Microphysical Data and Models

BRYAN A. BAUM

NASA Langley Research Center, Hampton, Virginia

ANDREW J. HEYMSFIELD

National Center for Atmospheric Research, Boulder, Colorado*

PING YANG

Texas A&M University, College Station, Texas

SARAH T. BEDKA

Cooperative Institute for Meteorological Satellite Studies, Madison, Wisconsin

(Manuscript received 29 July 2004, in final form 3 June 2005)

ABSTRACT

This study reports on the use of in situ data obtained in midlatitude and tropical ice clouds from airborne sampling probes and balloon-borne replicators as the basis for the development of bulk scattering models for use in satellite remote sensing applications. Airborne sampling instrumentation includes the two-dimensional cloud (2D-C), two-dimensional precipitation (2D-P), high-volume precipitation spectrometer (HVPS), cloud particle imager (CPI), and NCAR video ice particle sampler (VIPS) probes. Herein the development of a comprehensive set of microphysical models based on in situ measurements of particle size distributions (PSDs) is discussed. Two parameters are developed and examined: ice water content (IWC) and median mass diameter D_m. Comparisons are provided between the IWC and D_m values derived from in situ measurements obtained during a series of field campaigns held in the midlatitude and tropical regions and those calculated from a set of modeled ice particles used for light-scattering calculations. The ice particle types considered in this study include droxtals, hexagonal plates, solid columns, hollow columns, aggregates, and 3D bullet rosettes. It is shown that no single habit accurately replicates the derived IWC and D_m values, but a mixture of habits can significantly improve the comparison of these bulk microphysical properties. In addition, the relationship between D_m and the effective particle size D_{eff}, defined as 1.5 times the ratio of ice particle volume to projected area for a given PSD, is investigated. Based on these results, a subset of microphysical models is chosen as the basis for the development of ice cloud bulk scattering models in Part II of this study.

1. Introduction

We report on progress toward the development of a set of microphysical and optical models for use in the retrieval of global ice cloud properties by the Moderate Resolution Imaging Spectroradiometer (MODIS) on the National Aeronautics and Space Administration (NASA) Earth Observing System *Terra* and *Aqua* platforms. Our goal is to form bulk scattering models for the purpose of retrieving ice cloud properties globally from satellite imagery, specifically cloud optical thickness and particle size. What is unique about this new formulation is the inclusion of more than 1000 in situ horizontally averaged particle size distributions (PSDs) obtained from a variety of field campaigns in both midlatitude and tropical locales in addition to an extensive set of theoretical scattering properties for a variety of particle sizes and habits (i.e., particle shapes).

* The National Center for Atmospheric Research is sponsored by the National Science Foundation.

Corresponding author address: Dr. Bryan A. Baum, NASA LaRC, 1225 W. Dayton St., Madison, WI 53706.
E-mail: bryan.baum@ssec.wisc.edu

In general, the microphysical models upon which most satellite ice cloud retrieval groups base their analyses make limited use of the in situ data that have been collected over the past several decades. For example, the cirrus scattering models used operationally since 1999 by the MODIS Atmospheres Team are based solely on midlatitude cirrus measurements (Baum et al. 2000; King et al. 2004). These version-1 (V1) models are based on ice particle size distributions that have been discretized into five size bins and use a mixture of four habits: hollow columns, plates, 2D bullet rosettes, and aggregates. The habit distribution is the same for all models and is a function only of particle size. The V1 cirrus models are used in conjunction with a radiative transfer model to develop static libraries of radiances/reflectances that are a function of optical thickness and particle size.

The development of a new set of midlatitude cirrus microphysical and scattering models was explored in Nasiri et al. (2002). The models used the same habits as were used for the V1 models but employed greater particle size discretization (27 size bins, as compared with the original 5 size bins used in the operational MODIS cirrus models) and a characterization of the particle habit (shape) distributions. With the scattering property database developed for 27 size bins, the largest particle size bin was centered at 3500 μm.

A relevant question to ask is how well these midlatitude cirrus models represent the geographical and seasonal range of ice cloud properties found globally. One major difference between midlatitude and tropical cirrus is that the tropical cirrus formed near centers of convection tend to contain more crystals of larger sizes than do the midlatitude, synoptically generated cirrus. For most synoptically generated midlatitude cirrus, the largest crystal sizes measured are typically less than 1500 μm. Larger particles tend to settle out quickly because of the relatively low updraft velocities in the cloud layer. Updraft velocities in convection associated with the generation of tropical cirrus tend to be much higher, however, and the in situ measurements show that many large particles are typically present even in the uppermost regions of the cloud. This situation is also generally true for midlatitude ice clouds formed in areas of strong convection.

Recent research with tropical cirrus in situ data has raised many issues, two of which are addressed in this work. The first issue pertains to our discretization of a particle size distribution into a number of bins for the purposes of performing theoretical scattering calculations. Measurements of particle sizes in tropical cirrus, especially in the anvils of a cumulonimbus system near the convective cores, show the presence of particles that are up to centimeters in size. The presence of larger particles (i.e., >3500 μm) in a PSD is important for realistic representation of the ice water content but may have limited impact on the scattering and absorption properties.

Another issue is the choice of a model representation of a habit appropriate for use in calculating the scattering properties of the extremely large crystals that form in areas of strong updrafts. The aggregate appears to be the most complex of the habits assumed in the scattering calculations, but, as we will show later, this particular habit does not represent tropical ice particles adequately. For the scattering calculations, the aggregate is composed of a random number of columns attached to each other (Yang et al. 2000; Baum et al. 2000). Independent assessment of large, complex ice particles suggests that this idealization of the aggregate may be expedient from the perspective of light-scattering calculations but is not the most realistic representation of such particles.

The basis for our research is the in situ data, specifically vertical distributions in particle size and habit, derived during various field missions (Heymsfield et al. 2002, 2003). The habits for which theoretical scattering calculations are available include hollow and solid hexagonal columns, three-dimensional (3D) bullet rosettes, aggregates, hexagonal plates, and droxtals. The droxtal has 20 facets and is designed to represent small quasi-spherical particles (Yang et al. 2003; Zhang et al. 2004). For each of the habits, a library has been developed of the scattering properties (including scattering phase function, single-scattering albedo, extinction coefficient, extinction efficiency, asymmetry parameter, and size information) over an extended range of particle sizes (2–9500 μm). The library's spectral coverage includes 234 wavelengths between 0.4 and 13 μm as follows: 0.4–1.0 μm in increments of 0.01 μm, 1.20–1.70 μm in increments of 0.01 μm, 1.80–1.95 μm in increments of 0.01 μm, 2.05–2.20 μm in increments of 0.01 μm, 3.45–4.05 μm in increments of 0.05 μm, 8.10–8.95 μm in increments of 0.05 μm, and 10.00–13.00 μm in increments of 0.05 μm.

In addition to the bulk scattering properties, the ice cloud bulk scattering models include ice water content (IWC) and two different characterizations of particle size. The first is the effective particle size, which is based on the ensemble particle volume divided by the particle projected area for a given particle size and habit distribution. The effective particle size is used most commonly in descriptions of bulk scattering properties for a given PSD. The second is the median mass diameter D_m, defined as the size that divides the mass

content of a particle size distribution in half. For a given value of D_m, one-half of the mass is in particles of smaller size and one-half resides in the larger particles. The D_m is more commonly used in prognostic schemes in general circulation models to characterize the bulk microphysical properties such as IWC and ice mass precipitation.

Section 2 discusses the data and models used for the analyses. A comparison of scattering models at several wavelengths is provided in section 3. Results from a comparison of in situ and calculated IWC and D_m values are provided in section 4, and section 5 summarizes the study. Based on the in situ particle size and habit distributions developed herein, a comprehensive set of scattering models is developed in Baum et al. (2005, hereinafter Part II) for the various types of ice clouds measured during the various field campaigns.

2. In situ microphysical ice cloud data

a. Field campaigns

A summary of the in situ data is presented in Table 1. Field campaigns located in the midlatitudes include the First International Satellite Cloud Climatology Project Regional Experiments in Madison, Wisconsin, in 1986 (FIRE-I) and Coffeyville, Kansas in 1991 (FIRE-II). Midlatitude cirrus measurements were obtained by National Center for Atmospheric Research (NCAR) aircraft during FIRE-I.

Particle size distributions and habit imagery from FIRE-II were obtained from balloon-borne replicators (Miloshevich and Heymsfield 1997) over a size range from about 10 to between 500 and 1000 μm, with a resolution of about 2 μm. The replicators measure size distributions and yield particle imagery and cross-sectional areas reliably even for the smallest particles in the 10–20-μm diameter range. The continuous replicator observations are averaged over vertical distances of about 300 m (Heymsfield and Miloshevich 2003).

Another midlatitude dataset was derived in the spring of 2000 during an Atmospheric Radiation Measurement Program (ARM) intensive observation period near Lamont, Oklahoma. The University of North Dakota (UND) Citation aircraft was used to obtain in situ measurements for the ARM campaign. The midlatitude cirrus generally had temperatures ranging from $-65°$ to $-20°$C, with values of visible optical thickness τ_{vis} between 0.5 and 7. The extinction is derived from the particle cross-sectional areas as measured by the particle probes together with number concentration; optical thickness is derived from integrating over the Lagrangian spiral descents (Heymsfield et al. 2003). These ice cloud layers formed in association with synoptic-scale lifting.

In 1998 and 1999, four field campaigns were conducted under the auspices of the Tropical Rainfall Measuring Mission (TRMM). Although the purpose of the campaigns was to evaluate the performance of the TRMM radar and radiometer retrieval algorithms, they also provided validation data for TRMM mesoscale and regional-scale models, as well as in situ data from deep

TABLE 1. Data sources for in situ measurements of ice cloud properties. Probe size ranges are 40–1000 μm for 2D-C, 200–6400 μm for 2D-P, 200–6100 μm for HVPS, 20–2000 μm for CPI, 10–800 μm for replicator, and 20–200 μm for VIPS.

Date	Location	Alt (m)	Temperature (°C; min, max)	Instruments	IWC (g m^{-3}; min, max)	D_m (μm; min, max)
19 Oct 1986	Madison, WI	8631–6992	−41, −28	2D-C, 2D-P	2.60×10^{-3}, 2.87×10^{-2}	322, 554
22 Oct 1986	Madison, WI	8590–5435	−36, −15	2D-C, 2D-P	3.15×10^{-3}, 9.42×10^{-2}	308, 995
25 Oct 1986	Madison, WI	8292–5601	−35, −15	2D-C, 2D-P	2.06×10^{-2}, 1.04×10^{-1}	425, 1003
25 Oct 1986	Madison, WI	7652–5788	−30, −16	2D-C, 2D-P	2.32×10^{-3}, 1.98×10^{-1}	287, 1151
28 Oct 1986	Madison, WI	7956–6262	−34, −21	2D-C, 2D-P	6.05×10^{-3}, 1.02×10^{-1}	487, 1173
1 Nov 1986	Madison, WI	8964–6190	−43, −21	2D-C, 2D-P	1.98×10^{-3}, 1.80×10^{-2}	198, 431
1 Nov 1986	Madison, WI	8800–5041	−41, −18	2D-C, 2D-P	5.70×10^{-3}, 9.08×10^{-2}	231, 698
2 Nov 1986	Madison, WI	7786–4992	−36, −19	2D-C, 2D-P	8.39×10^{-3}, 8.63×10^{-2}	259, 683
25 Nov 1991	Coffeyville, KS	9809–7313	−52, −33	Replicator	2.30×10^{-4}, 4.98×10^{-2}	78, 223
26 Nov 1991	Coffeyville, KS	9816–6131	−54, −24	Replicator	1.12×10^{-4}, 1.49×10^{-2}	82, 220
5 Dec 1991	Coffeyville, KS	12 316–9381	−63, −40	Replicator	2.90×10^{-3}, 1.41×10^{-2}	97, 254
5 Mar 2000	Lamont, OK	9969–8661	−52, −40	2D-C, 2D-P, CPI	2.51×10^{-3}, 3.39×10^{-2}	139, 249
9 Mar 2000	Lamont, OK	9398–6699	−49, −27	2D-C, 2D-P, CPI	1.59×10^{-3}, 1.63×10^{-1}	196, 1323
18 Aug 1999	Kwajalein	8423–5745	−25, −6	2D-C, HVPS, CPI	3.20×10^{-3}, 6.13	333, 2450
22 Aug 1999	Kwajalein	11 125–7340	−49, −19	2D-C, HVPS, CPI	4.60×10^{-2}, 1.17	173, 2703
23 Aug 1999	Kwajalein	10 403–6099	−42, −9	2D-C, HVPS, CPI	4.86×10^{-3}, 5.47	136, 680
11 Sep 1999	Kwajalein	10 057–4510	−39, 0	2D-C, HVPS, CPI	3.80×10^{-2}, 1.08	150, 4255
26 Jul 2002	Nicaragua	15 161–13 000	−76, −58	2D-C, VIPS	3.79×10^{-4}, 2.75×10^{-3}	50, 105

tropical cirrus and stratiform precipitating clouds. The tropical data used in this study were obtained from the UND Citation flights conducted in Kwajalein, Marshall Islands [the Kwajalein Experiment (KWAJEX)], in 1999 (Stith et al. 2002, 2004). The tropical cloud temperatures ranged from −70° to 0°C, with τ_{vis} values between 20 and 30, and the clouds formed in association with deep convection.

In addition, recent high-quality measurements have been acquired during the Cirrus Regional Study of Tropical Anvils and Cirrus Layers (CRYSTAL) Florida Area Cirrus Experiment (FACE) during a series of flights by the NASA WB57 aircraft and the UND Citation in 2002. The CRYSTAL FACE data used in this study were obtained from the WB57 flight track recorded off the coast of Nicaragua and provide data from extremely cold cirrus (from −76° to −58°C).

Imaging probes provide the aircraft-based size spectra measurements (Heymsfield et al. 2002, 2003, 2004). The Particle Measuring Systems, Inc., (PMS) two-dimensional cloud (2D-C) probes provide sizes from about 50 to 1000 μm. The 2D-C resolution is 25 μm for FIRE-I but is 33 μm for the other campaigns listed in Table 1. A PMS two-dimensional precipitation (2D-P) probe measured larger particle sizes (from 1000 to more than 3000 μm) for the FIRE-I and ARM campaigns, with resolutions of 100 μm for FIRE-I and 200 μm for ARM. In addition, for the TRMM field campaign large particle sizes from 1 to more than 30 mm were obtained from a Stratton Park Engineering Company (SPEC) high-volume precipitation spectrometer (HVPS) probe with a resolution of 0.2 mm. A SPEC cloud particle imager (CPI) provided imagery for the ARM and TRMM campaigns over a range of sizes from 20 to 2000 μm with a 2-μm resolution. The CPI probe provides spectacular imagery of the ice particles, but its accuracy in measuring PSDs has yet to be established. Therefore, the CPI data were not used to evaluate the numbers of small crystals in the PSDs. The forward-scattering spectrometer probe (FSSP) data, which provide particle sizes from 2 to 30 μm, are thought to be unreliable for particles having sizes greater than several hundred micrometers (Heymsfield et al. 2004) because of possible particle breakup in the probe inlet and are not used in this study. The NCAR video ice particle sampler (VIPS) was used in part to obtain size distributions in the 20–200-μm range for the Nicaragua CRYSTAL case.

Further discussion of the measurement techniques and analysis of field campaign data are provided in Heymsfield et al. (2002, 2004) and Heymsfield and Miloshevich (2003).

b. Particle size distributions

Each PSD is parameterized in the form of a gamma distribution (e.g., Kosarev and Mazin 1991; Mitchell 1991; Heymsfield et al. 2002) of the form

$$n(D) = N_0 D^{\mu} e^{-\lambda D}, \quad (1)$$

where D is the particle maximum dimension, $n(D)$ is the particle concentration per unit volume, N_0 is the intercept, λ is the slope, and μ is the dispersion. This relationship reduces to an exponential distribution when $\mu = 0$. The values for the intercept, slope, and dispersion were derived for each PSD by matching three moments; in this case, the first, second, and sixth moments were chosen because this set provided the best fit over the measured particle size range (Heymsfield et al. 2002).

The data are filtered by cloud temperature to ensure that the particle phase is ice. Spectra are used from clouds that are colder than −25°C. Data from an ice detector probe support the view that these particles are ice. The gamma fit parameters have been developed for more than 4000 PSDs measured in ice clouds in the midlatitudes, Tropics, and subtropics, but 1117 PSDs remain after filtering by cloud temperature, with a breakdown by field campaign shown in Table 2. Our focus is predominantly on data collected from Lagrangian spiral descents from the top to base of the ice cloud layers so that 1) optical depths can be estimated from the particle size distributions, 2) changes in particle size by height within the cloud column can be examined (a measurement more relevant to what a satellite observes), and 3) changes in particle shape in the vertical direction can be assessed. Each PSD from the aircraft observations represents a vertical depth within the cloud of about 30 m, and each replicator point represents roughly 300 m in the vertical direction. With Lagrangian descent spirals, the broadening of the PSDs may be attributed to the evolution of the size distributions through aggregation rather than size sorting.

TABLE 2. Number of particle size distributions for each field campaign. Note that the total sample set has been filtered by the requirement that the cloud temperature be colder than −25°C. A total of 1117 PSDs are used in this study.

Field campaign	Location	No. of PSDs
FIRE-I	Madison, WI	246
FIRE-II	Coffeyville, KS	22
ARM	Lamont, OK	390
TRMM	Kwajalein, Marshall Islands	418
CRYSTAL FACE	Nicaragua/Caribbean	41

c. *Inference of D_m and IWC from in situ measurements*

The two bulk cloud characteristics of interest in this study, D_m and IWC, are directly related to the PSDs (i.e., number concentration as a function of particle diameter) and the particle mass as a function of size. Recent studies examine the derivation of these bulk cloud properties from aircraft data (e.g., Heymsfield et al. 2002, 2004; Heymsfield and Miloshevich 2003) and will be discussed only briefly here. The IWC was deduced from the in situ measurements from a mass dimension relationship and the size distributions. The mass dimension relationship was deduced from direct measurements of the IWC for clouds that were similar to those sampled during the various field programs (Heymsfield et al. 2004). The IWC calculations are thought to be accurate to better than 25%. The D_m was derived both analytically by assuming the gamma size distribution fit parameters (Heymsfield et al. 2002) and from the distribution of particle mass with size as derived from the size distributions and the mass dimension relationship.

The D_m (cm) and IWC (g m^{-3}) for the gamma PSDs can be represented analytically by the following relationships:

$$D_m = \frac{b + \mu + 0.67}{\lambda} \quad \text{and} \tag{2}$$

$$\text{IWC} = \frac{aN_0\Gamma(b + 1 + \mu)}{\lambda^{(b+1+\mu)}}, \tag{3}$$

where N_0, λ, and μ are defined in Eq. (1) and Γ is the gamma function. For TRMM data, $a = 5050$ and $b = 2.1$. The CRYSTAL data are best represented by the TRMM coefficients. For the midlatitude data (ARM, FIRE-I, and FIRE-II), $a = 6590$ and $b = 2.3$.

d. *Comparison of gamma PSDs with MODIS version-1 PSDs*

Figure 1a shows a sample of PSDs based upon Eq. (1). The PSD from CRYSTAL FACE, which involves a flight track off the coast of Nicaragua that sampled the coldest cloud in our data, displays the narrowest size distribution. Both the ARM and FIRE-II data were from fairly cold midlatitude cirrus and have similar PSD shapes. The FIRE-I cirrus data typically come from warmer cirrus and display a broader range of particle sizes than do the colder clouds. The tropical cirrus shown in the TRMM PSD is typical of the anvil associated with deep convection and exhibits more of an exponential size distribution behavior. In general, there are more particles across the entire size range than for the other cirrus data. The TRMM stratiform ice cloud layers are convectively generated. The ice water contents are approximately an order of magnitude larger than those for the other cases. The PSDs accordingly manifest higher concentrations of particles. The high

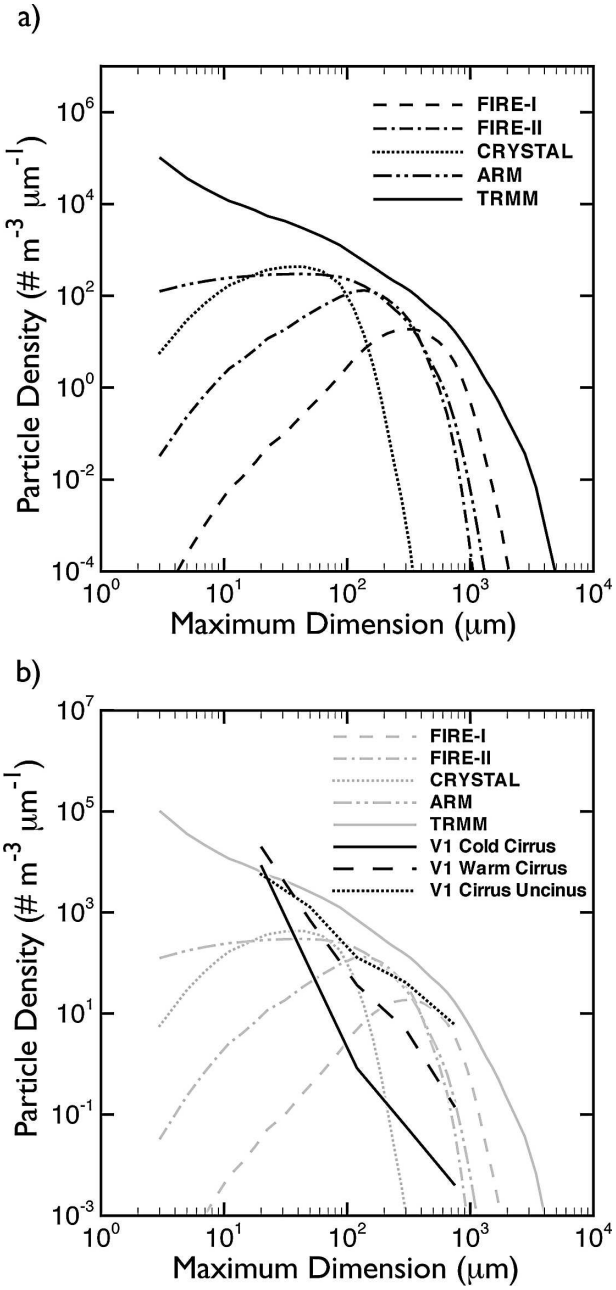

FIG. 1. (a) Sample of PSDs selected from the various field experiments. The FIRE-I, FIRE-II, ARM, and CRYSTAL data have the appearance of the more general "gamma" distribution, whereas the TRMM PSD follows an exponential particle distribution. (b) In addition to the gamma-fit PSDs shown in (a) there are three PSDs from the V1 microphysical models: cold cirrus, warm cirrus, and cirrus uncinus.

concentration of small particles is likely due to ice particles ejected from the anvils that have been nucleated through homogeneous freezing.

The set of 12 MODIS V1 PSDs is provided in Table 3. Three of these V1 models (cold cirrus, warm cirrus, and cirrus uncinus) are shown in Fig. 1b for comparison with the models shown in Fig. 1a. In the V1 size distributions, the total particle concentrations do not vary drastically. The mass is focused in the small sizes and, as it happens, where the sampling is the most problematic. It is evident that the V1 PSDs do not adequately capture the particle size variability shown in Fig. 1a. We note that the V1 PSD spectra were derived in part from 1D-C/1D-P probe data. Even with current sampling techniques, determining the appropriate number of very small particles to use in a PSD is an issue. The influence of the small particles on the single-scattering albedo and asymmetry factor is shown in Part II of this study.

3. Model ice particle microphysical properties

Extensive libraries of microphysical and single-scattering properties have been developed for a variety of ice crystal habits, including droxtals (Yang et al. 2003), two- and three-dimensional bullet rosettes, solid and hollow columns, plates, and aggregates (Yang et al. 2000). Calculations are performed for droxtals only up to 200 μm in maximum dimension. For all other habits, scattering properties are developed for particle sizes ranging from 2 to 9500 μm. The scattering calculations for all habits assume a random orientation. Microphysical properties for each habit include length, width, aspect ratio, volume, and projected area as a function of maximum dimension.

As shown in Fig. 1, the PSDs from tropical cirrus are much broader than for midlatitude synoptic cirrus, meaning that more large particles are present in the distributions, and in higher concentrations. To accommodate the broader size distributions, the number of size bins has been increased from 27 (Nasiri et al. 2002) to 45, with the primary change being higher resolution for the largest particle sizes between 1000 and 9500 μm. For each of the habits, a library has been developed of the scattering properties (including scattering phase function, single-scattering albedo, extinction coefficient, extinction efficiency, asymmetry parameter, and size information) for a range of satellite wavelengths between 0.4 and 13 μm. The scattering properties are discussed further in Part II.

For simulated ice particles, Fig. 2 shows volume as a function of maximum dimension. For particles having $D_{\max}$ less than 200 μm (Fig. 2a), the droxtals have the highest volume and the aggregates and bullet rosettes tend to have the lowest volume. For habits with $D_{\max}$ between 200 and 2000 μm (Fig. 2b), aggregates tend to have the highest volume and the 3D bullet rosettes have the lowest volume. For $D_{\max}$ greater than 2000 μm, aggregates have the highest volume and columns have the lowest volume.

4. Results

There are two issues that will have a significant affect on the bulk scattering/absorption properties of the ice cloud models: 1) the number of small particles, perhaps underrepresented because of in situ sampling issues, and 2) the number of large particles sometimes present near the cloud top in regions of strong convection, that is, regions with relatively strong updrafts that tend to loft ice particles to high altitudes. The large particles tend to have less influence on the single-scattering properties in the visible and near-infrared bands than do the more numerous small particles, but they are

TABLE 3. The 12 MODIS V1 particle size distributions (Ci is cirrus; Cs is cirrostratus).

Cirrus model	D_{eff} (μm)	20 μm (No. m^{-3} μm^{-1})	50 μm (No. m^{-3} μm^{-1})	120 μm (No. m^{-3} μm^{-1})	300 μm (No. m^{-3} μm^{-1})	750 μm (No. m^{-3} μm^{-1})
Cold Ci	13.4	8600	75.16	0.8367	0.058 67	0.003 994
Ci at $T = -60$°C	19.1	3034	86.38	2.877	0.081 75	0.002 323
Cs	28.9	6700	975.8	32.43	1.497	0.000
Warm Ci	39.4	20 050	702.8	36.94	4.807	0.1414
Ci at $T = -20$°C	50.0	10 320	669.1	48.99	3.175	0.2058
Ci at $T = -40$°C	56.0	7398	612.5	56.67	4.692	0.2005
1 Nov 1986	64.0	807.6	189.4	41.83	4.813	0.040 92
2 Nov 1986	80.0	789.2	214.1	47.49	17.50	0.1921
22 Oct 1986	94.8	1434	302.6	36.63	11.31	0.5857
28 Oct 1986	97.1	956.6	244.1	37.69	10.51	0.5789
25 Oct 1986	101.3	1847	425.6	55.94	18.62	1.191
Ci uncinus	117.8	5710	1280	129.4	41.10	5.976

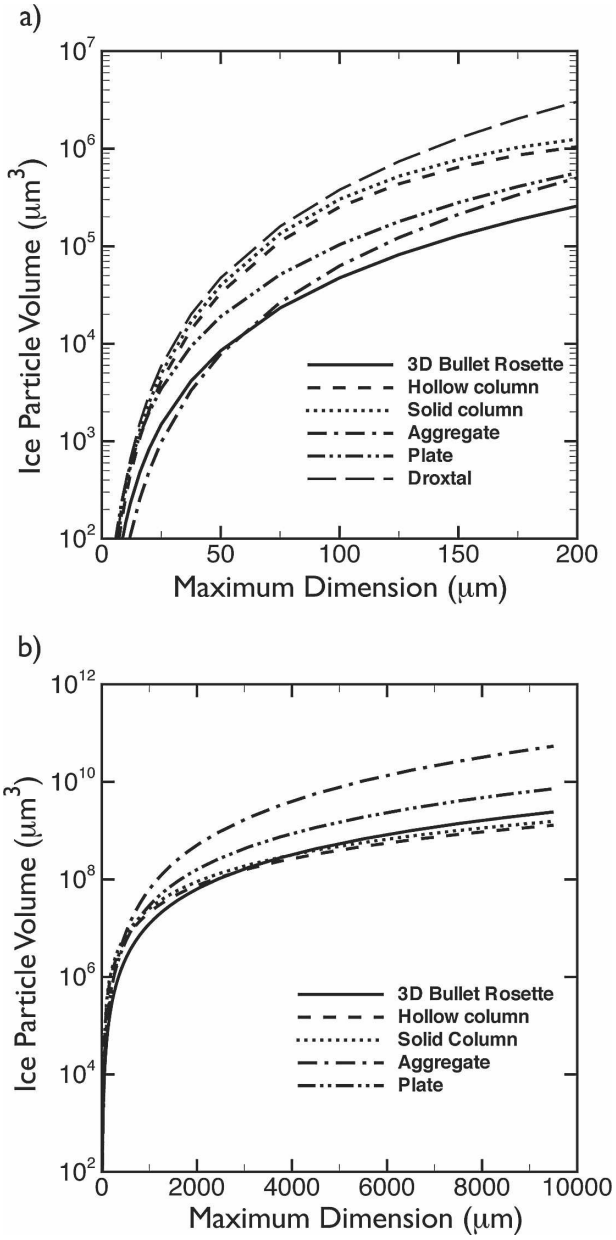

FIG. 2. Ice crystal volume as a function of habit and crystal maximum dimension D_{max} (a) for small particles only and (b) over the full range of particle sizes. Droxtal properties have been calculated for small particles only ($D_m < 200$ μm).

important for inferring the ice water content. Given the in situ D_m and IWC values for the size distributions deduced from the midlatitude and tropical field campaign data, it is a straightforward matter to compare these with the same parameters calculated from distributions of the simulated ice particles.

The total volume of ice per unit volume of air for a given distribution is given by

$$V_{TOT} = \sum_{h=1}^{M} \left[\int_{D_{min}}^{D_{max}} V_h(D)\, n(h,D)\, dD \right], \qquad (4)$$

where D_{min} and D_{max} describe the minimum and maximum particle sizes in the distribution, $n(h, D)$ is the number distribution of a specific particle habit h for size D, and $V_h(D)$ is the volume of the habit h for size D. The total mass is obtained by multiplying the total volume by the bulk ice density (0.917 g cm^{-3}).

A first set of calculations is performed using the assumption of a single ice particle habit in the integration over each particle size distribution. Because the ice volume per volume of air is a function of both habit and D_{max}, but especially ice particle concentration (which is proportional to the concentration intercept parameter N_0), one might expect that the relationship between IWC (which is proportional to N_0) and D_m (which is not proportional to N_0) could vary substantially given a range of particle size and habit distributions.

Results are presented assuming that the ice particle habit is entirely composed of aggregates (Fig. 3), 3D bullet rosettes (Fig. 4), or solid columns (Fig. 5). In all three figures, the upper and lower panels show a comparison between values of IWC and D_m deduced from the in situ measurements (section 2c, henceforth referred to as "in situ" in the figures) and those derived from the simulated ice particles (section 3, henceforth referred to as "calculated" in the figures). When the particles are all aggregates (Fig. 3), the IWC values from the midlatitude field campaigns (FIRE-I, FIRE-II, and ARM) tend to be distinct from the tropical data (CRYSTAL FACE and TRMM). The calculated IWC values for CRYSTAL FACE are lower than those deduced from the in situ data; the opposite is true for the PSDs having the highest IWC values obtained from TRMM. The calculated values of D_m tend to be much higher than those estimated from the in situ data, however.

When 3D bullet rosettes are employed (Fig. 4), the bifurcation in D_m between the midlatitude and tropical data is still apparent. The D_m values computed from TRMM using the 3D bullet rosettes are uniformly higher than those inferred from the in situ data. For all PSDs, however, the in situ IWC values are higher than those calculated using the 3D bullet rosettes. Our interpretation of these results is that the 3D bullet rosette formulation lacks the volume and, hence, mass that is observed in the in situ data. Of our simulated ice particle habits, the 3D bullet rosette is the only one that leads generally to an underestimate of IWC and an overestimate of D_m for the set of PSDs.

Figure 5 shows the same comparison but with solid hexagonal columns used for the ice particles. The as-

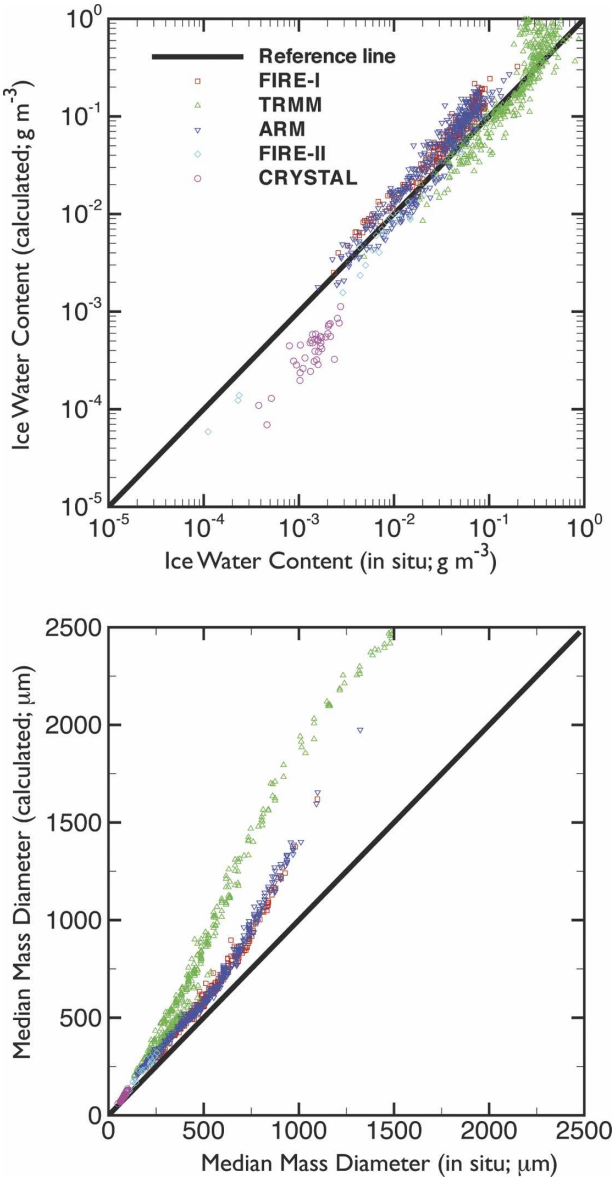

FIG. 3. Comparison of in situ and calculated IWC and D_m for each of the size distributions obtained from the FIRE-I, FIRE-II, ARM, TRMM, and CRYSTAL field campaigns. The habit distribution is as follows: $D_{\max} < 60$ μm, 100% droxtals; $D_{\max} > 60$ μm, 100% aggregates.

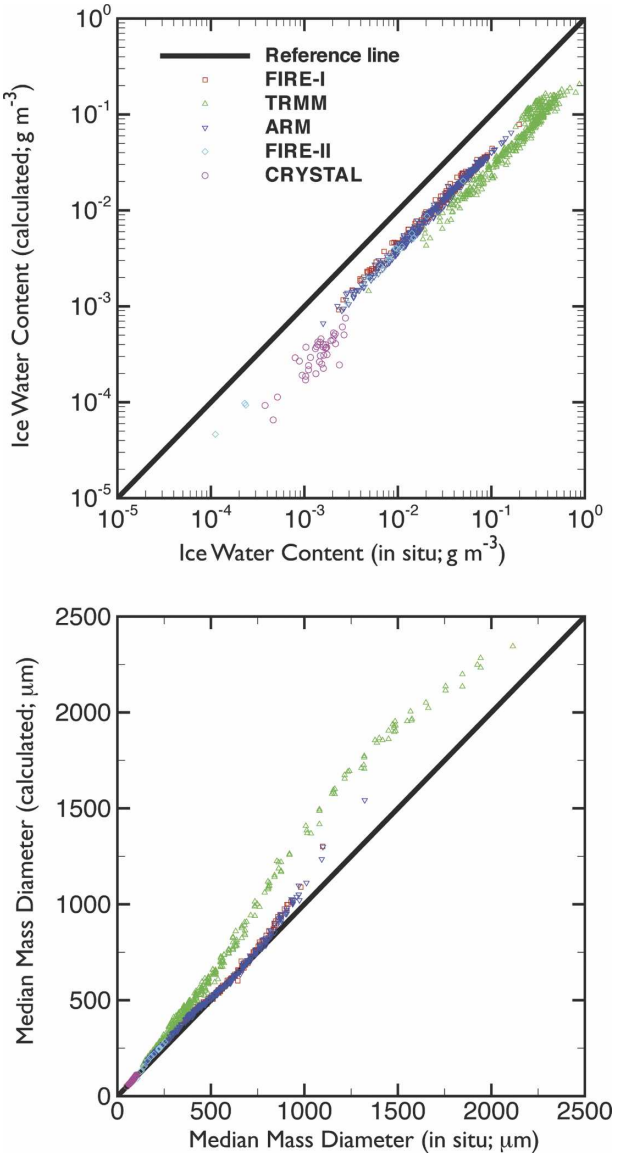

FIG. 4. As in Fig. 3, but the habit distribution is as follows: $D_{\max} < 60$ μm, 100% droxtals; $D_{\max} > 60$ μm, 100% 3D bullet rosettes.

sumption of a single columnar habit for the derivation of ice cloud scattering libraries has been reported by Minnis et al. (1998), for example. The calculated IWC values tend to be higher by approximately 30% than those inferred from the measurements for most of the midlatitude cloud data, but the TRMM data tend to compare more closely. For D_m values of less than 500 μm, the calculated values tend to agree closely with those inferred from the measurements. At higher D_m values, the in situ data have higher values than those calculated.

Based on these results, there may be some cause for optimism for developing a single habit distribution that will increase the agreement between observed and calculated values for IWC and D_m. Given that the use of a single habit in the PSDs cannot provide adequate comparisons with the IWC and D_m values inferred from the in situ data, we developed the following approach to find a suitable habit mixture. Each PSD was divided into four domains based on particle maximum dimension as follows: $D_{\max} < 60$ μm, $60 < D_{\max} < 1000$ μm, $1000 < D_{\max} < 2000$ μm, and $D_{\max} > 2000$ μm. The

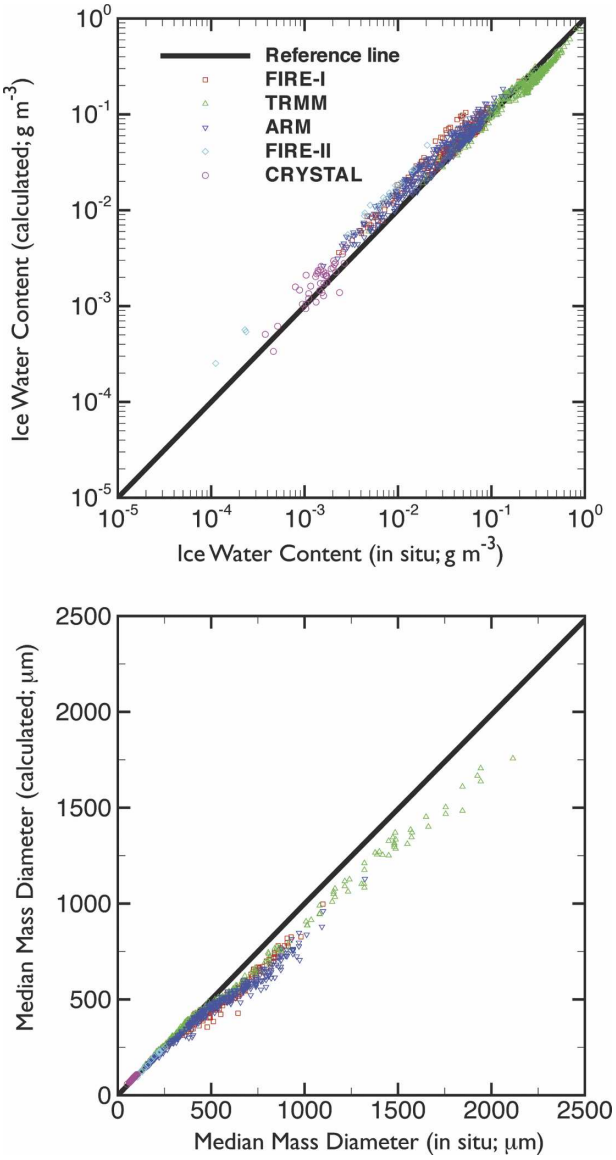

FIG. 5. As in Fig. 3, but the habit distribution is as follows: $D_{max} < 60$ μm, 100% droxtals; $D_{max} > 60$ μm, 100% solid columns.

goal was to use all habits with the following restrictions: droxtals were used to represent only the smallest particles, that is, those with D_{max} less than 60 μm, plates were used for intermediate-sized particles no larger than 1000 μm, and both solid and hollow columns were used for particles no larger than 2000 μm. Observations have shown that neither plates nor columns tend to occur at sizes much larger than 1500–2000 μm (Ono 1969; Auer and Veal 1970). Aggregrates were used only for particles larger than 1000 μm. Based on these restrictions and size domains, an initial (and arbitrary) set of habit percentages was adjusted to improve the comparison of calculated and inferred (in situ) IWC and D_m values. While there may be many combinations of habits that optimize the comparison of measured values with calculated values, we formulated one such distribution as follows: $D_{max} < 60$ μm is 100% droxtals; $60 < D_{max} < 1000$ μm is 15% 3D bullet rosettes, 50% solid columns, and 35% plates; $1000 < D_{max} < 2000$ μm is 45% hollow columns, 45% solid columns, and 10% aggregates; and $D_{max} > 2000$ μm is 97% 3D bullet rosettes and 3% aggregates. The resulting comparison of calculated and measured IWC and D_m values is provided in Fig. 6. At higher IWC values, the measured values for TRMM tend to be lower than the calculated values but are within a factor of 2. Overall, there is general agreement in IWC and D_m over four orders of magnitude (from 10^{-4} to 10^{0} g m^{-3}).

One could argue that a habit distribution could be derived for each flight track that minimizes the difference between the in situ and calculated IWC and D_m values. Perhaps this approach could be investigated in future work. The primary purpose of this work is to provide a way to estimate particle size and, hence, IWP from remote sensing data that is more consistent with field measurements. We suggest that D_m may be a more useful parameter for numerical weather and climate modelers than some measure of effective particle size. Nonetheless, if the retrievals are performed using a consistent set of models that are traceable to in situ measurements, it will be more straightforward to validate the data products.

For satellite retrievals, a common definition for the effective size of any particular PSD is provided by the effective diameter D_{eff}, which is proportional to the ratio of the total volume to the total projected area for a given particle size distribution. After Foot (1988) and Francis et al. (1994), D_{eff} is defined as

$$D_{\text{eff}} = \frac{3}{2} \frac{\sum_{h=1}^{M} \left[\int_{D_{\min}}^{D_{\max}} V_h(D)\, n(h,D)\, dD \right]}{\sum_{h=1}^{M} \left[\int_{D_{\min}}^{D_{\max}} A_h(D)\, n(h,D)\, dD \right]}, \qquad (5)$$

where $A_h(D)$ is the projected area (per unit volume of air) of the particle habit h for size D.

Because both D_m [Eq. (2)] and D_{eff} are independent of the particle number concentration, there should be some relationship between the two. Figure 7 provides a comparison between D_m and D_{eff}. The highest values of both D_{eff} and D_m occur for TRMM data, as one might expect given that the clouds are convective in origin. The range of D_{eff} is from 38 to 240 μm, and the range of D_m is from 48 to 2010 μm.

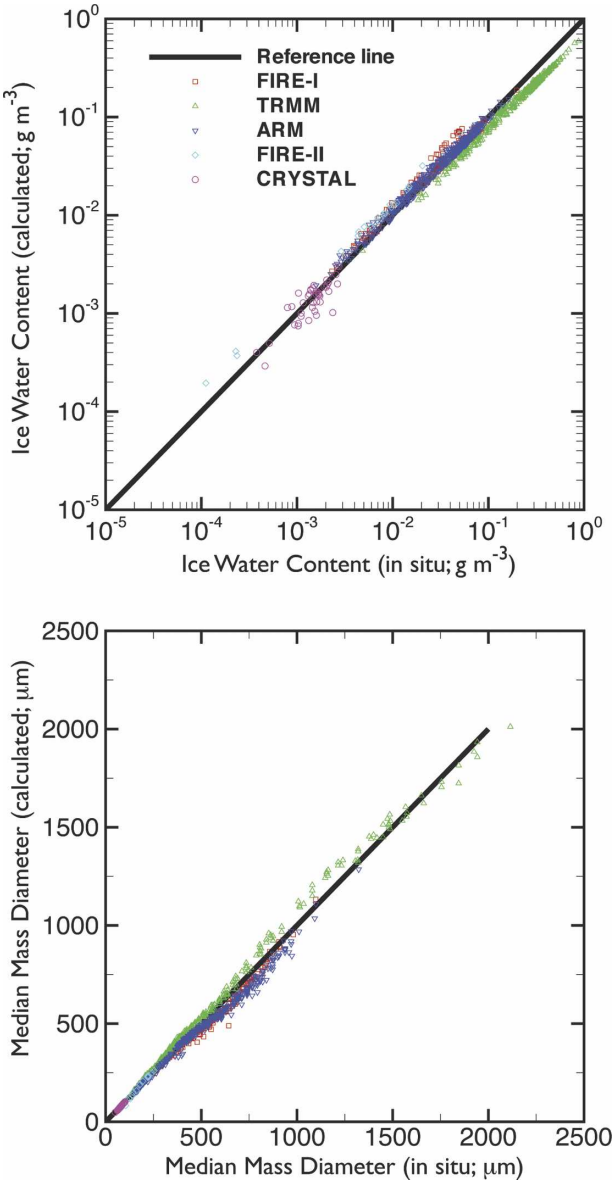

FIG. 6. As in Fig. 3, but the habit distribution is as follows: $D_{max} < 60$ μm, 100% droxtals; $60 < D_{max} < 1000$ μm, 15% 3D bullet rosettes, 50% solid columns, and 35% plates; $1000 < D_{max} < 2000$ μm, 45% hollow columns, 45% solid columns, and 10% aggregates; $D_{max} > 2000$ μm, 97% 3D bullet rosettes and 3% aggregates.

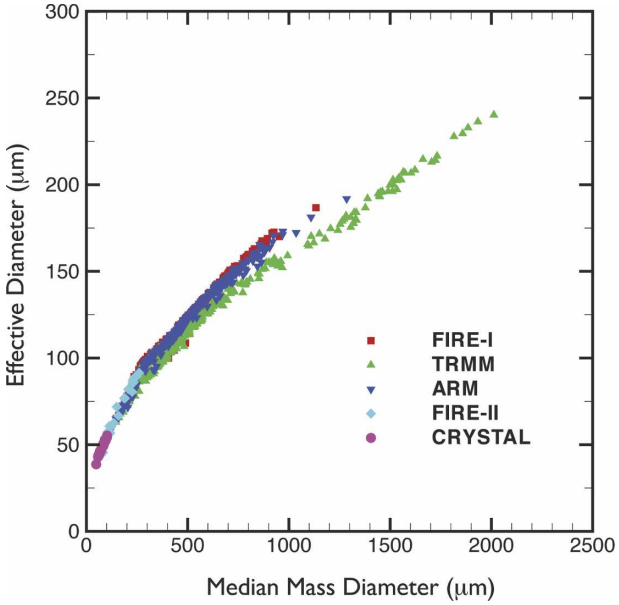

FIG. 7. Comparison of effective diameter D_{eff} and median mass diameter D_m.

5. Summary

This study reports on the use of aircraft in situ data obtained from midlatitude and tropical ice clouds as the basis for the development of scattering models for use with satellite remote sensing applications. Herein the development of a comprehensive set of microphysical models is described. Two parameters are developed: ice water content and median mass diameter. Comparisons are provided between the IWC and D_m values obtained from in situ measurements during a series of field campaigns held in the midlatitude and tropical regions and those calculated from a set of modeled ice crystals used for light-scattering calculations. The modeled ice crystals include droxtals, hexagonal plates, solid columns, hollow columns, aggregates, and 3D bullet rosettes. We show that no single habit model accurately replicates the IWC and D_m values inferred from the in situ measurements, but a habit mixture can significantly improve the comparison of derived with modeled microphysical properties. Based on these results, a subset of microphysical models is chosen as the basis for the development of ice cloud bulk scattering models in Part II of this study.

One observation regarding the use of the simulated habits is that the aggregate is a very dense particle, with the highest volume (and hence mass) at large crystal sizes. A habit distribution that relies primarily on aggregates will overestimate both D_m and IWC. The 3D bullet rosette has the least volume/mass at intermediate particle sizes and tends to underestimate the IWC for both midlatitude and tropical size distributions. A difference between the bullet rosette and the aggregate is that, although IWC is underestimated, the D_m is overestimated with respect to the in situ data. Of the habits, the solid column compares most favorably to measurements of D_m and IWC. However, we show that a mixture of habits can improve the comparison of the in situ values with calculated values.

In addition, we investigate the relationship between D_m and the effective particle size D_{eff}, defined as 1.5 times the ratio of ice particle volume to projected area for a given PSD. There is a monotonic relationship between the two parameters for the ARM, FIRE-I, FIRE-II, and CRYSTAL FACE data, but the TRMM data diverge slightly. The range of D_m values is much greater than the range for D_{eff} for the set of PSDs used in this study.

Acknowledgments. This research was sponsored by the NASA Science Directorate (formerly the Office of Earth Science). The authors specifically acknowledge the support and encouragement of Drs. Hal Maring and Donald Anderson of the NASA Radiation Program at NASA Headquarters. Doctor Yang's research is supported additionally by a National Science Foundation (NSF) CAREER Award research grant (ATM-0239605).

REFERENCES

Auer, A. H., Jr., and D. L. Veal, 1970: The dimension of ice crystals in natural clouds. *J. Atmos. Sci.,* **27,** 919–926.

Baum, B. A., D. P. Kratz, P. Yang, S. Ou, Y. Hu, P. F. Soulen, and S.-C. Tsay, 2000: Remote sensing of cloud properties using MODIS Airborne Simulator imagery during SUCCESS. I. Data and models. *J. Geophys. Res.,* **105,** 11 767–11 780.

——, P. Yang, A. J. Heymsfield, S. Platnick, M. D. King, Y.-X. Hu, and S. T. Bedka, 2005: Bulk scattering properties for the remote sensing of ice clouds. Part II: Narrowband models. *J. Appl. Meteor.,* **44,** 1896–1911.

Foot, J. S., 1988: Some observations of the optical properties of clouds: II Cirrus. *Quart. J. Roy. Meteor. Soc.,* **114,** 145–164.

Francis, P. N., A. Jones, R. W. Saunders, K. P. Shine, A. Slingo, and Z. Sun, 1994: An observational and theoretical study of the radiative properties of cirrus: Some results from ICE'89. *Quart. J. Roy. Meteor. Soc.,* **120,** 809–848.

Heymsfield, A. J., and L. M. Miloshevich, 2003: Parameterizations for the cross-sectional area and extinction of cirrus and stratiform ice cloud particles. *J. Atmos. Sci.,* **60,** 936–956.

——, A. Bansemer, P. R. Field, S. L. Durden, J. Stith, J. E. Dye, W. Hall, and T. Grainger, 2002: Observations and parameterizations of particle size distributions in deep tropical cirrus and stratiform precipitating clouds: Results from in situ observations in TRMM field campaigns. *J. Atmos. Sci.,* **59,** 3457–3491.

——, S. Matrosov, and B. A. Baum, 2003: Ice water path–optical depth relationships for cirrus and precipitating cloud layers. *J. Appl. Meteor.,* **42,** 1369–1390.

——, A. Bansemer, C. Schmitt, C. Twohy, and M. R. Poellot, 2004: Effective ice particle densities derived from aircraft data. *J. Atmos. Sci.,* **61,** 982–1003.

King, M. D., S. Platnick, P. Yang, G. T. Arnold, M. A. Gray, J. C. Riédi, S. A. Ackerman, and K. N. Liou, 2004: Remote sensing of liquid water and ice cloud optical thickness and effective radius in the Arctic: Application of airborne multispectral MAS data. *J. Atmos. Oceanic Technol.,* **21,** 857–875.

Kosarev, A. L., and I. P. Mazin, 1991: An empirical model of the physical structure of upper layer clouds. *Atmos. Res.,* **26,** 213–228.

Miloshevich, L. M., and A. J. Heymsfield, 1997: A balloon-borne continuous cloud particle replicator for measuring vertical profiles of cloud microphysical properties: Instrument design, performance, and collection efficiency analysis. *J. Atmos. Oceanic Technol.,* **14,** 753–768.

Minnis, P., D. P. Garber, D. F. Young, R. F. Arduini, and Y. Takano, 1998: Parameterization of reflectance and effective emittance for satellite remote sensing of cloud properties. *J. Atmos. Sci.,* **55,** 3313–3339.

Mitchell, D. L., 1991: Evolution of snow-size spectra in cyclonic storms. Part II: Deviations from the exponential form. *J. Atmos. Sci.,* **48,** 1885–1899.

Nasiri, S. L., B. A. Baum, A. J. Heymsfield, P. Yang, M. Poellot, D. P. Kratz, and Y. Hu, 2002: Development of midlatitude cirrus models for MODIS using FIRE-I, FIRE-II, and ARM in situ data. *J. Appl. Meteor.,* **41,** 197–217.

Ono, A., 1969: The shape and riming properties of ice crystals in natural clouds. *J. Atmos. Sci.,* **26,** 138–147.

Stith, J. L., J. E. Dye, A. Bansemer, A. J. Heymsfield, D. A. Grainger, W. A. Petersen, and R. Cifelli, 2002: Microphysical observations of tropical clouds. *J. Appl. Meteor.,* **41,** 97–117.

——, J. A. Haggerty, A. J. Heymsfield, and C. A. Grainger, 2004: Microphysical characteristics of tropical updrafts in clean conditions. *J. Appl. Meteor.,* **43,** 779–794.

Yang, P., K. N. Liou, K. Wyser, and D. Mitchell, 2000: Parameterization of the scattering and absorption properties of individual ice crystals. *J. Geophys. Res.,* **105,** 4699–4718.

——, B. A. Baum, A. J. Heymsfield, Y. X. Hu, H.-L. Huang, S.-C. Tsay, and S. Ackerman, 2003: Single scattering properties of droxtals. *J. Quant. Spectrosc. Radiat. Transfer,* **79-80,** 1159–1169.

Zhang, Z., P. Yang, G. W. Kattawar, S.-C. Tsay, B. A. Baum, Y. X. Hu, A. J. Heymsfield, and J. Reichardt, 2004: Geometric optics solution for the scattering properties of droxtal ice crystals. *Appl. Opt.,* **43,** 2490–2499.